Robust correlated magnetic moments in end-modified graphene nanoribbons

Honet, Antoine; Henrard, Luc; Meunier, Vincent

Published in:
Carbon Trends

DOI:
10.1016/j.cartre.2024.100377

Publication date:
2024

Document Version
Publisher's PDF, also known as Version of record

Carbon Trends 16 (2024) 100377

Contents lists available at ScienceDirect

Carbon Trends

journal homepage: www.elsevier.com/locate/cartre

Robust correlated magnetic moments in end-modified graphene nanoribbons

Antoine Honet [a,*], Luc Henrard [b], Vincent Meunier [c]

[a] Université libre de Bruxelles (ULB), Spectroscopy, Quantum Chemistry and Atmospheric Remote Sensing (SQUARES), Brussels, Belgium
[b] Department of Physics, Namur Institute of Structured Materials, University of Namur, Rue de Bruxelles 51, 5000 Namur, Belgium
[c] Department of Engineering Science and Mechanics, The Pennsylvania State University, State College, PA, USA

ARTICLE INFO

Keywords:
Graphene nanorribons
Magnetic moments
Correlation
Hubbard model
Mean-field approximation
GW approximation
Topological end states

ABSTRACT

We conduct a theoretical examination of the electronic and magnetic characteristics of end-modified 7-atom wide armchair graphene nanoribbons (AGNRs). Our investigation is performed within the framework of a single-band Hubbard model, beyond a mean-field approximation. First, we carry out a comprehensive comparison of various approaches for accommodating di-hydrogenation configurations at the AGNR ends. We demonstrate that the application of an on-site potential to the modified carbon atom, coupled with the addition of an electron, replicates phenomena such as the experimentally observed reduction of the bulk-states (BS) gap. These results for the density of states (DOS) and electronic densities align closely with those obtained through a method explicitly designed to account for the orbital properties of hydrogen atoms. Furthermore, our study enables a clear differentiation between magnetic moments already described in a mean-field (MF) approach, which are spatially confined to the same sites as the topological end-states (ES), and correlation-induced magnetic moments, which exhibit localization along all edges of the AGNRs. Notably, we show the robustness of these correlation-induced magnetic moments relative to end modifications, within the scope of the method we employ.

1. Introduction

Graphene nanoribbons (GNRs) have been the subject of many studies in the last two decades both theoretically [1–7] and experimentally [8–16]. This interest in GNRs is explained in part by the possibility of inducing a band gap in graphene nanosystems while extended graphene has a zero band gap [1–3,17]. GNRs are also interesting because, for example, finite-sized armchair graphene nanoribbons (AGNRS) and AGNRS heterojunctions are known to host topological states [18–20]. AGNRs of different widths can now be synthesized using a bottom-up approach with atomic precision [8–16]. This allows not only the study of the fundamental properties of specific AGNRs but also the engineering of GNRs with well-defined electronic properties.

In the process of synthesizing 7-atom-wide AGNRs (7-AGNRs), different possible end terminations have been observed [9]. The influence of termination on the bandgap value was studied in Ref. [14] both experimentally and theoretically using the density functional theory (DFT) and tight-binding (TB) methods. In that study, the end modifications include dehydrogenation and di-hydrogenation of the central carbon (C) atom at the zigzag ends. It was observed that di-hydrogenation of the two ends leads to the reduction of the bulk-state (BS) bandgap, defined as the bandgap between states that are not topological end-states (ES). This BS bandgap reduction was reproduced using a single-band TB model and removing the C atom sites where the di-hydrogenation took place since they cannot contribute with an electron to the π-system [14,21].

Furthermore, doped GNRs can be produced by introducing substituent to C atoms such as nitrogen (N) or boron (B) [22–24]. It is possible to describe such substitution in the TB framework, adapting the number of electrons and setting an on-site potential at the substituent atomic sites. One electron is added (resp., removed), and the on-site potential is set to a negative (resp., positive) value for a N (resp,. B) substitution [25–29].

Magnetic moments in graphene nanostructures are important for technological applications. They are often studied using a mean-field (MF) approximation of the Hubbard model [4,21,30–33]. When electron–electron effects are included, a correlation part has to be included in the magnetic moment expression, which accounts for the non-decoupling of double occupancies [34–38]. The relation between topological states energy renormalization and local magnetic moments was recently investigated in GNR heterojunctions using a many-body GW approximation for inclusion of correlation effects [36]. In this reference, it was shown that the magnetic moments in MF are predicted to be spatially localized exactly where the zero-energy states are located while they are located along all edges of the GNRs and not only at

* Corresponding author.
E-mail address: antoine.honet@ulb.be (A. Honet).

https://doi.org/10.1016/j.cartre.2024.100377
Received 13 October 2023; Received in revised form 24 May 2024; Accepted 5 July 2024
Available online 10 July 2024

the location of the zero-energy states in the GW approximation, with a larger range of values in the system. Because magnetic moments are strongly affected by correlation, we study them in this article in pristine and end-modified 7-AGNRs. We investigate the spatial localization of the magnetic moments in MF and GW approximation by changing the number of electrons and the on-site potential at the modified atomic sites at the end of the graphene nanoribbon.

The rest of this paper is organized as follows: we start by reviewing the models and methods used throughout this study in Section 2. We then compare in more details different ways of modeling di-hydrogenation within the Hubbard model framework in Section 3. Next, we adopt a common model for all end-modification scenarios to study the magnetic moments induced by topological ES and by correlation effects in Section 5. We also study the robustness of these magnetic moments against end-modifications of the AGNRs, contrasting them with topologically-induced and correlated magnetic moments.

2. Models and methods

2.1. Single-band Hubbard model for extended graphene and nanoflakes with edges passivated with hydrogen atoms

In extended graphene, each C atom is bound to three other C atoms, leading to sp^2 hybridization. As a result, each C atom contributes one p_z electron to the π system, allowing the use of the single-band TB or Hubbard model. In the case of graphene nanoflakes, such as finite-size AGNRs, single-band models can be used if one assumes that each C atom at the edges is passivated by exactly one H atom. The C atoms at the edges are then bound to two other C atoms and one H atom, leading to sp^2 hybridization. We therefore model these systems with TB or Hubbard Hamiltonians at half-filling, *i.e.*, with the number of electrons being equal to the number of C atoms.

The single-band Hubbard Hamiltonian up to nearest-neighbor hopping terms reads:

$$\hat{H}_{Hubbard} = \sum_{i,\sigma} \epsilon_{i,\sigma} \hat{c}^{\dagger}_{i\sigma} \hat{c}_{i\sigma} - t \sum_{\langle ij\rangle,\sigma} (\hat{c}^{\dagger}_{i\sigma} \hat{c}_{j\sigma} + c.c.) + U \sum_{i} \hat{n}_{i\uparrow} \hat{n}_{i\downarrow}, \tag{1}$$

where $\epsilon_{i,\sigma}$ are the on-site potentials, t (resp. U) is the hopping (resp. interaction) parameter, $\hat{c}^{\dagger}_{i\sigma}$ (resp. $\hat{c}_{i\sigma}$) is a creation (resp. destruction) operator of an electron at atomic site i with spin σ and $\hat{n}_{i\sigma} = \hat{c}^{\dagger}_{i\sigma}\hat{c}_{i\sigma}$ is the density operator (of electrons on atomic site i and with spin σ). The $\langle\ \rangle$ sign under the summation symbol indicates that the sum runs over all pairs of nearest neighbors. In the event that all atoms are equivalent, as assumed in pure carbon systems, all on-site potentials are equal and they only lead to a global shift in energy. We therefore arbitrarily set them to zero. Typical values for the hopping parameter in graphene are around or slightly below 3 eV [4,17,39] and we took $t = 2.7$ eV throughout this work. We used $U = 2t$, which is a typical realistic value for carbon nanostructures [7,36,39].

2.2. Modeling N or B substitutions

Starting the TB Hamiltonian of pure C systems described in Eq. (1), one can model the substitution of one C atom by an N or a B atom by changing the on-site potential ϵ at the substitutional site and by changing the number of electrons. Since N atoms have one electron more than C atoms, one electron is added in the π system for each N substitution. The on-site potential for the N atoms is set to a negative value of several eV [25–29], meaning that it attracts more electrons than the other C atoms, accounting for the different atomic numbers. The case of substitution for B is modeled analogously by removing one electron from the π system and setting a positive on-site value of several eV [25–29]. The resulting model Hamiltonian reads:

$$\hat{H}_{subst} = \epsilon_{N/B} \sum_{\alpha\in subst,\sigma} \hat{c}^{\dagger}_{\alpha\sigma}\hat{c}_{\alpha\sigma} - t \sum_{\langle ij\rangle,\sigma} (\hat{c}^{\dagger}_{i\sigma}\hat{c}_{j\sigma} + c.c.) + U \sum_{i} \hat{n}_{i\uparrow}\hat{n}_{i\downarrow}, \tag{2}$$

where the α index runs over all substitutional sites and the $\epsilon_{N/B}$ is the N or B on-site potential.

2.3. Modeling di-hydrogenation

There exist several ways to model the effect of di-hydrogenation on a given C atomic site in graphene. The first one, called *C-removing*, consists in removing the affected sites of the TB/Hubbard model [14,21]. The electron that the C atom shared with the π system in the single-hydrogen passivated case is now used to bind to the second hydrogen. The π-electron of the C atom then does not contribute anymore to the system and can be ignored. The Hamiltonian operator in this case is simply the one described by Eq. (1) where the sums run over the C atomic sites except the ones where di-hydrogenation occurs. The number of electrons remains equal to the number of C atoms, *i.e.* the models are considered at half-filling.

A second way of modeling di-hydrogenation is by considering H atomic sites as potential atomic sites for the electron to be localized and therefore by adding H orbitals and associated hopping/on-site parameters in the Hamiltonian. Therefore, we refer to this approach using the *H-orbitals* denomination. One H atom comes with one electron such that the total number of electrons is the number of C atomic site plus one for each site of di-hydrogenation. The Hamiltonian accounting for di-hydrogenated in nanographene samples is therefore given by the following equation:

$$\hat{H} = \hat{H}_{Hubbard} + \hat{H}_{H}, \tag{3}$$

where $\hat{H}_{Hubbard}$ is given at Eq. (1) and $\hat{H}_H$ is a H-related Hamiltonian given by:

$$\hat{H}_H = \epsilon_H \sum_{\alpha,\sigma} \hat{h}^{\dagger}_{\alpha\sigma}\hat{h}_{\alpha\sigma} + t_h \sum_{\alpha,\sigma} (\hat{h}^{\dagger}_{\alpha\sigma}\hat{c}_{h_\alpha,\sigma} + c.c.), \tag{4}$$

where index α runs over all H atoms added for di-hydrogenation, $\hat{h}_{\alpha\sigma}$ (resp., $\hat{h}^{\dagger}_{\alpha\sigma}$) is the annihilation (resp., creation) operator of an electron on the H atom labeled α with spin σ, the notation $\hat{c}_{h_\alpha}$ denotes the annihilation operator on the C atom to which the H label α is adsorbed, ϵ_h is the on-site parameter at the H site, and t_h is the hopping parameter linking the H atom and the C atom where H is added. These parameters were chosen to be $\epsilon_h = -t/16$ and $t_h = 2t$ [40].

We considered a third way of modeling di-hydrogenation. As previously, the basic idea is that an electron should be added to the system and forced to stay close to the C atom that hosts the di-hydrogenation site. According to these principles, we propose to model di-hydrogenation by adding an electron in the system and keeping the initial system composed of only C atoms, *i.e.* not removing any C sites nor introducing any H sites. Instead, the localization around the C atoms subject to di-hydrogenation is modeled by setting a large negative value for its on-site potential [31]. We name this third method *C-on-sites*. The model Hamiltonian thus reads:

$$\hat{H}_{o-s} = \epsilon_{o-s} \sum_{\alpha\in\{C_H\},\sigma} \hat{c}^{\dagger}_{\alpha\sigma}\hat{c}_{\alpha\sigma} - t \sum_{\langle ij\rangle,\sigma} (\hat{c}^{\dagger}_{i\sigma}\hat{c}_{j\sigma} + c.c.) + U \sum_{i} \hat{n}_{i\uparrow}\hat{n}_{i\downarrow}, \tag{5}$$

where the α index runs over all C atomic sites that are subject to di-hydrogenation (the ensemble of these C sites is written $\{C_H\}$.

One can easily see that the Hamiltonians described by Eqs. (2) and (5) are identical up to the order of magnitude of the on-site potential values. This similarity could allow one to simulate di-hydrogenation and substitution in a unified framework. In Section 3 we compare the

different approaches for modeling di-hydrogenation and we show that the *C-on-sites* method can capture features that are also observed in the two other methods for large enough negative on-site values. This allows us to consider only the *C-on-sites* method for the di-hydrogenation modeling in an attempt to unify the description of end-modifications.

2.4. MF approximation of the Hubbard term

The interaction term (third term of Eq. (1)) is often treated in a MF approximation to model graphene's electronic properties [4,33,41,42]. The MF approximation consists of decoupling the product of two density operators in the interaction term $\hat{n}_{i\uparrow}\hat{n}_{i\downarrow}$. The approximation is then between the density operator of one spin and mean density of the opposite spin:

$$\hat{H}_{Hub,MF} = \hat{H}_{TB} + \sum_i U(\hat{n}_{i\uparrow}\langle\hat{n}_{i\downarrow}\rangle + \langle\hat{n}_{i\uparrow}\rangle\hat{n}_{i\downarrow}), \tag{6}$$

where $\langle\hat{n}_{i\sigma}\rangle$ is the mean value of the operator $\hat{n}_{i\sigma}$. By adopting such an approximation, the products of deviations with the mean densities and a constant shift in the Hamiltonian are neglected [43]. The Hamiltonian of Eq. (6) has to be solved self-consistently, starting from an initial guess for the mean densities and updating them at each step, where a new Hamiltonian is diagonalized.

2.5. GW approximation

The GW approximation is a beyond-MF approximation that includes some correlation effects *via* dynamically-screened interaction. The approximation was recently applied to the Hubbard model in the context of graphene nanostructures [7,36,39]. The GW approximation is based on Hedin's equations [44] that are approximated according to the vertex function that leads to Dyson's equation:

$$G^R(\omega) = G_0^R(\omega) + G_0^R(\omega)\Sigma^R(\omega)G^R(\omega), \tag{7}$$

where G_0^R is the non-interacting retarded Green's function (computed using the MF solution), G^R is the exact retarded Green's function, and Σ^R is the retarded self-energy. Each of these quantities are matrix quantities in the atomically localized and spin basis and Dyson's equation has to be understood as a matrix equation. In the GW approximation, the self-energy is approximated by the (matrix) product of the Green's function and the screened potential W, computed within the random phase approximation (RPA), see *e.g.*, Refs. [36], [39] and [38] for a description of the full equations and theoretical framework. As it is common practice, we work in natural units, such that $\hbar = 1$ and ω is in energy units.

Similarly to the MF approximation, the GW approximation operates in a self-consistent manner, updating G^R and Σ^R at each step until convergence is reached for the Green's function.

2.6. (Local) density of states, local densities and magnetic moments

From the Green's functions, we define the spectral function: $A_{i\sigma,j\sigma'}(\omega) = -2\,\mathrm{Im}(G^R_{i\sigma,j\sigma'}(\omega))$. The local density of states (LDOS, written $n_{i\sigma}(\omega)$) is proportional to the diagonal terms of the spectral function and the density of states (DOS, written $D(\omega)$) is the sum of all LDOS:

$$n_{i\sigma}(\omega) = \frac{1}{2\pi}A_{i\sigma,i\sigma}(\omega) \tag{8}$$

and

$$D(\omega) = \sum_{i\sigma} n_{i\sigma}(\omega). \tag{9}$$

The local electronic densities are found by integrating the local density of states weighted in frequency by the Fermi–Dirac statistics:

$$n_{i\sigma} = \int_{-\infty}^{+\infty} \mathrm{d}\omega\, n_{i\sigma}(\omega) f_{FD}(\omega), \tag{10}$$

where $f_{FD}(\omega)$ is the Fermi–Dirac statistics.

Finally, the local magnetic moments are defined as [36]:

$$\begin{aligned}\langle\hat{m}_i^2\rangle &= \langle(\hat{n}_{i\uparrow} - \hat{n}_{i\downarrow})^2\rangle \\ &= \Big(n_{i\uparrow} + n_{i\downarrow} - 2\,d_i\Big),\end{aligned} \tag{11}$$

where $d_i = \langle\hat{n}_{i\uparrow}\hat{n}_{i\downarrow}\rangle$ are the double occupancies and $\langle(\hat{n}_{i\sigma})^2\rangle = \langle\hat{n}_{i\sigma}\rangle = n_{i\sigma}$ for Fermions.

The double occupancies are found in the Green's function formalism using an adaptation of the Galitskii–Migdal formula:

$$d_i = \frac{-1}{U}\sum_{k,\sigma,\bar{\sigma}}\int\frac{\mathrm{d}\omega}{2\pi} f_{FD}(\omega-\mu)\,\mathrm{Im}\{\Sigma^{R,tot}_{i\bar{\sigma},k\sigma}(\omega)G^R_{k\sigma,i\bar{\sigma}}(\omega)\}, \tag{12}$$

where $\Sigma^{R,tot}$ is the total retarded self-energy. Since in our case the GW approximation is constructed with the MF approximation as a starting point, the retarded self-energy in Eq. (7) does not account for the MF self-energy, which therefore must be included in the total self-energy of Eq. (12). The total self-energy is then written

$$\Sigma^{R,tot} = \Sigma^R + \Sigma^{MF,R}, \tag{13}$$

where $\Sigma^{MF,R}$ is the MF self-energy.

Splitting the double occupancies of Eq. (12) according to the total self-energy expression (Eq. (13)) leads to:

$$d_i = d_i^{corr} + d_i^{MF}, \tag{14}$$

where d_i^{corr} (resp. d_i^{MF}) is the correlation (resp., MF-like) part of the double occupancies found by replacing $\Sigma^{R,tot}$ by Σ^R (resp., $\Sigma^{R,MF}$) in Eq. (12).

The MF self-energy is diagonal in spin and expressed using MF mean densities [45,46]:

$$\Sigma^{MF,R}_\sigma(\omega) = U\ \mathrm{diag}(n^{MF}_{1,\bar{\sigma}}, n^{MF}_{2,\bar{\sigma}}, \dots, n^{MF}_{N,\bar{\sigma}}), \tag{15}$$

with $\bar{\sigma} = -\sigma$.

Using Eq. (15), the MF-like double occupancies of Eq. (14) can be written as:

$$d_i^{MF} = \frac{1}{2}(n^{MF}_{i,\uparrow}n_{i,\downarrow} + n^{MF}_{i,\downarrow}n_{i,\uparrow}). \tag{16}$$

In the MF approximation, double occupancies reduce to the MF-like ones and are given by $d_i = d_i^{MF} = n^{MF}_{i,\uparrow}n^{MF}_{i,\downarrow}$, leading to magnetic moments equals to:

$$\langle(\hat{m}_i^{MF})^2\rangle = n^{MF}_{i\uparrow} + n^{MF}_{i\downarrow} - 2n^{MF}_{i\uparrow}n^{MF}_{i\downarrow}, \tag{17}$$

according to Eq. (11).

2.7. Numerical methods

The TB, MF and GW computations are achieved using the Hubbard_GW code [47]. A broadening parameter [39] of $10^{-3}\,\frac{E_H}{t}$ (with $E_H = 27.21$ eV the Hartree energy) was used for the Green's functions and the number of frequencies in the grid varied from 2^{13} to 2^{14}. 2^{14} frequencies are needed for convergence for on-site potentials of $\epsilon = -20$ eV while 2^{13} was sufficient in other cases. The limits of the frequency grids were set to $\pm 16\pi t$ except for the fully H-passivated case for which $\pm 8\pi t$ were used. The structures were generated using the PYBINDING software [48]. The numerical visualization tools from PYBINDING package are used in Fig. 3 and in Figs. 1 and 2 of the SI.

3. Comparison between the different methods of modeling di-hydrogenation

We now study the different methods (*C-removing*, *H-orbitals*, and *C-on-sites*) presented in Section 2.3 for modeling di-hydrogenation in the case of end-modified 7-AGNRs. As far as the *H-orbitals* technique is concerned, we define effective mean density on a C atomic site hosting two H atoms as the sum of the mean densities on the C atomic

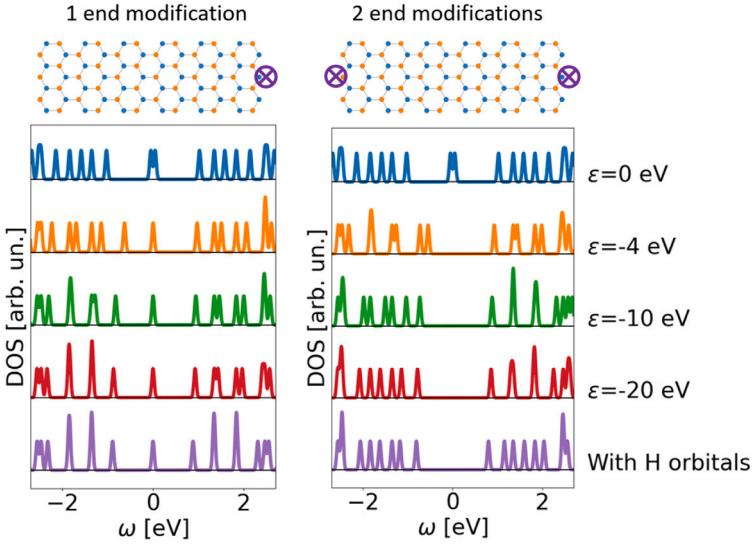

Fig. 1. DOS for 6 UC end-modified 7-AGNRs using the *C-on-sites* method with ϵ values of 0 eV, −4 eV, −10 eV and −20 eV (top four curves) and using the *H-orbitals* method (bottom curves), within a TB model (*i.e.* with $U = 0$) with $t = 2.7$ eV. All curves are shifted artificially for better visualization and the zero DOS levels are indicated with black lines. The left (resp., right) panel shows the DOS for AGNRs with one end (resp., two ends) modified. The locations of the end modifications are indicated on the structure with purple crossed circles. The structure plots were generated using the PYBINDING software [48]. All Fermi levels are aligned to 0 eV.

Table 1
BS energy gaps of 6 UC 7-AGNRs in the TB, MF, and GW approximations for a non end-modified AGNR, and symmetrically modified AGNRs (both ends) using the *C-removing* and *C-on-sites* methods with ϵ values set to 0 eV, −4 eV, −10 eV, and −20 eV. We used $t = 2.7$ eV and $U = 2t$.

	BS energy gaps [eV]		
	TB	MF	GW
No end-modification	1.97	2.12	2.1
C removing	1.58	1.59	1.75
$\epsilon = 0$ eV	1.98	1.99	2.04
$\epsilon = -4$ eV	1.43	1.24	1.27
$\epsilon = -10$ eV	1.56	1.53	1.69
$\epsilon = -20$ eV	1.58	1.58	1.74

site and on the additional H atom. This is further illustrated in the Supplementary Information (see Fig. 1 of the SI).

We first compare the *C-on-sites* and the *C-removing* methods, including TB computations similar to Ref. [14] in our comparison. In this reference, the authors showed experimentally that the BS gap is significantly reduced when the central C atoms of both ends of a 7-AGNR are di-hydrogenated. Moreover, they used TB computations and the C-removing modeling of di-hydrogenation to study the phenomenon and showed that this BS gap reduction is correctly reproduced. Table 1 reports the BS energy gaps of a finite-size 6 unit cells (UC) 7-AGNR (see illustration of the system on top of Fig. 1) in the TB, MF and GW approximation for the case of no end-modification as well as two end-modifications modeled using the *C-removing* method and the *C-on-sites* method with different on-sites values ranging from 0 eV to −20 eV. We see in the table that the experimentally observed BS gap reduction is reproduced in all three approximations when considering the *C-removing* method, reduced from $\sim$ 2–2.1 eV to $\sim$ 1.6–1.75 eV. When considering the C-on-sites method, the BS gaps are reduced significantly for intermediate on-site energies, (see $\epsilon = -4$ eV in Table 1), for all approximations (TB, MF and GW). They then increase to reach the ones predicted *via* the *C-removing* method for large negative ϵ values.

Moving on to the comparison between the *C-on-sites* and the *H-orbitals* methods within the TB model, Fig. 1 shows the DOS for 6 UC 7-AGNRs with one and two end(s) modified for the two methods. For the C-on-sites method, ϵ values of 0 eV, −4 eV, −10 eV and −20 eV are considered. We observe for both systems that the DOS obtained from the *C-on-sites* method converges towards the *H-orbitals* DOS when the magnitude of ϵ is increased. The agreement between the two methods for $\epsilon = -20$ eV in the *C-on-sites* method is remarkable, especially for the unoccupied states. From Fig. 1, an apparent electron–hole symmetry for the *H-orbitals* method is observed while not for the *C-on-sites* one. This could be understood by the fact that the Hubbard model on a bipartite lattice is known to present particle–hole symmetry at half-filling [49,50]. Indeed, taking the H-passivated case at half-filling as a starting point, the *H-orbitals* method introduces two new orbitals with one electron, leading to a system at half-filling and then to an electron–hole symmetry even if numerical errors cannot be avoided. At the opposite, the *C-on-sites* method introduces one electron but no new orbitals (only an on-site is incorporated to model the modification), leading to non half-filled system. The electron–hole symmetry can then be theoretically broken.

This very good agreement is confirmed by inspecting the local electronic densities of Eq. (10), shown in Fig. 2 for the same methods and parameter values. The densities are the effective densities for the *H-orbitals* method as illustrated in the Supplementary Information (see Fig. 1 of the SI). As in Fig. 2, the scale is rather extended due to the strong localization for some models, it is instructive to also compare the electronic densities not representing the sites of strong localization for better visualization of smaller variations. This is done in the SI in Fig. 2, which allows us to also conclude that the large negative limit for ϵ reproduces the *H orbitals* model well, showing a more uniform density.

In conclusion, key features of end-modified AGNRs such as the BS energy gap, the DOS, and the total electronic density can be described using the *C-on-sites* method with great agreement with the two other modeling methods in the large enough negative value limit for the on-site potentials. Therefore, we model di-hydrogenation *via C-on-sites* method in the following of the paper, adopting a unified framework to describe di-hydrogenation and N/B substituents at the ends of AGNRs.

4. DOS and local electronic densities

For the case of finite-size 7-AGNRs with H-passivation at the edges, we showed in a previously published paper that the GW approximation introduces an energy renormalization of the topological end states and slight changes in the total LDOS which are more significant in the spin-polarized LDOS [7]. Fig. 3 shows the DOS of end-modified 6 UC 7-AGNRs using −4 eV and −10 eV for end-modifications at one or two

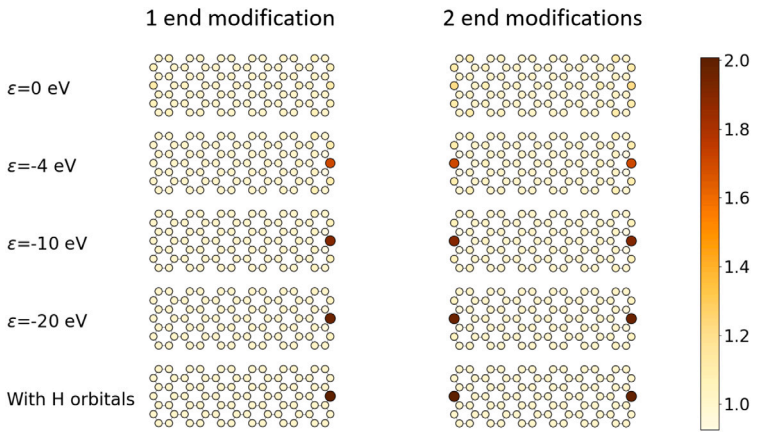

Fig. 2. Local electronic densities of the one-end (left) and two-end (right) modified AGNRs using the *C on-site* potential and *H orbitals* methods within a TB model (*i.e.* with $U = 0$) with $t = 2.7$ eV. The *C on-site* potential ϵ increases in magnitude when going downward in the panels and the last bottom panel is for the *H orbital* method.

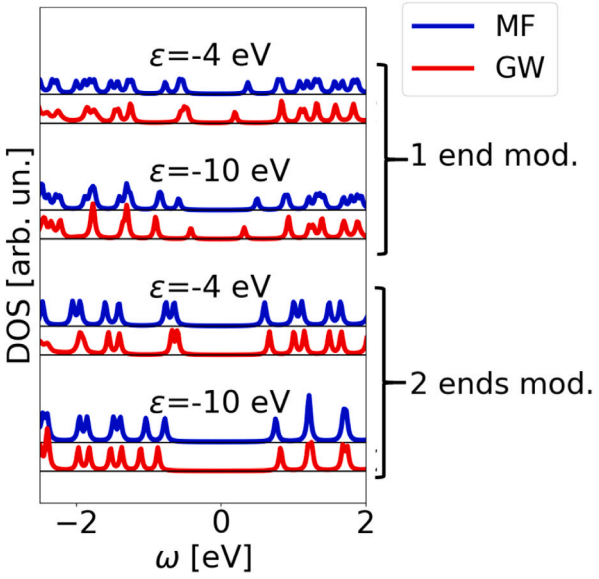

Fig. 3. DOS for 6 UC end-modified 7-AGNRs using *C-on-sites* method with ϵ values of −4 eV and −10 eV, in the MF (blue curves) and GW (red curves) approximations. All curves are shifted artificially for better visualization and the zero DOS levels are indicated with black lines. The top (resp., bottom) four curves show DOS for AGNRs with one end (resp., two ends) modified. All Fermi levels were aligned to 0 eV. We used $t = 2.7$ eV and $U = 2t$. (For interpretation of the references to color in this figure legend, the reader is referred to the web version of this article.)

end(s). As for the H-passivated case, we observe little changes between the MF and GW approximations, mainly energy renormalization of near-Fermi-level states.

When incorporating an end-modification, the spin-polarization at the modified end disappears as can be seen in Fig. 5. This could be understood as a consequence of the added electron occupying one more topological ES of the system. This is further illustrated in the SI in Fig. 4, where the magnetic moments of a two-electron doped system are shown, without any on-site potential. In the one-end modified case, the effect of GW approximation on the electronic density is again to reduce the spin polarization (near the unmodified end).

For GNRs that are modified symmetrically at both ends, all spin polarization is removed compared to the H-passivated case, resulting in a fully spin-symmetric electron density, as can be seen in Fig. 6. As a conclusion to this section, we can state that the MF and GW approximations lead to qualitatively similar results even if a more closely look shows that GW has the effect to renormalize the energies, mostly of the topological ES and to attenuate the spin polarization of the system, but there are still opposite spin accumulations at opposite ends in the H-passivated case (see Fig. 4), a single spin accumulation at the unmodified end for the one end-modified cases (see Fig. 5) and no spin polarization for the two end-modified cases (see Fig. 6).

5. Local magnetic moments in end-modified 7-AGNRs

Magnetic moments are quantities that are strongly affected by electronic correlation as pointed out in several studies using different methods for the inclusion of correlation [34,36,37]. Therefore in this section, we move to a quantification of correlation effects. In the MF approximation, magnetic moments can be calculated directly from mean occupations (Eq. (17)) while a correlated part must be included in the GW approximation.

The magnetic moments of 6 UC 7-AGNRs computed in the MF and GW approximations are displayed in Fig. 7 for the *H-passivated* case in (a) and *modified* cases with one and two ends using −4 eV in (b) and −10 eV in (c). We stress that the local magnetic moments presented in Fig. 7 are defined at Eq. (11) and are different quantities than the difference between spin up and spin down mean densities reported at the bottom of Figs. 4 and 5. For the *H-passivated* case (Fig. 7 a)), the local magnetic moments in the MF approximation are found at the two ends where the topological ES are located. The GW approximation predicts local magnetic moments in general larger than the MF approximation. The MF magnetic moments are $\sim$ 0.5–0.58 while the GW magnetic moments are $\sim$ 0.6–0.65. Moreover, the GW approximation predicts the largest magnetic moments along all the edges and not only at the two zigzag ends. These observations were already made for the H-passivated case considering AGNRs heterojunctions in a recent publication using MF and GW approximations [36].

For the one end-modified case (see the left illustrations shown in Fig. 7 (b) and (c)), the local magnetic moment at the site of modification decreases significantly when ϵ grows in absolute value, starting from $\sim$ 0.58 (MF) and $\sim$ 0.67 (GW) for the unmodified case to $\sim$ 0.13 (MF) and $\sim$ 0.12 (GW) when $\epsilon = -10$ eV. In the MF approximation, the magnetic moment at the opposite end (the unmodified one) decreases when ϵ increases in absolute value. Interestingly, the opposite behavior is observed in the GW approximation, resulting in a large local magnetic moment ($\sim$ 0.73) at the unmodified end of the one end-modified case with $\epsilon = -10$ eV.

For the two end-modified case (see the right illustrations in Fig. 7 (b) and (c)), we see a decrease in the local magnetic moment at the end-modified sites, similar to the one observed in the one end-modified case. In the MF approximation, all the unmodified sites present rather uniform magnetic moments. In contrast, the GW results show stronger magnetic on the (unmodified) edges.

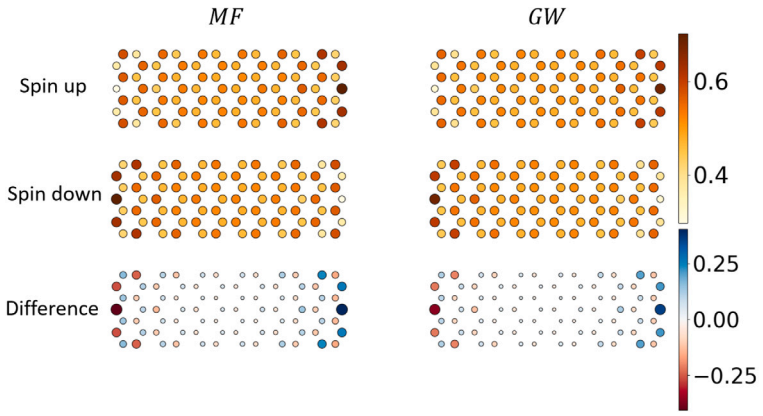

Fig. 4. Local electronic densities for H-passivated 6 UC 7-AGNRs. The left (resp., right) column shows the MF (resp., GW) results for spin-up and spin-down electrons (top and middle plots, respectively), as well as the difference between the two spin densities (bottom plots). We used $t = 2.7$ eV and $U = 2t$.

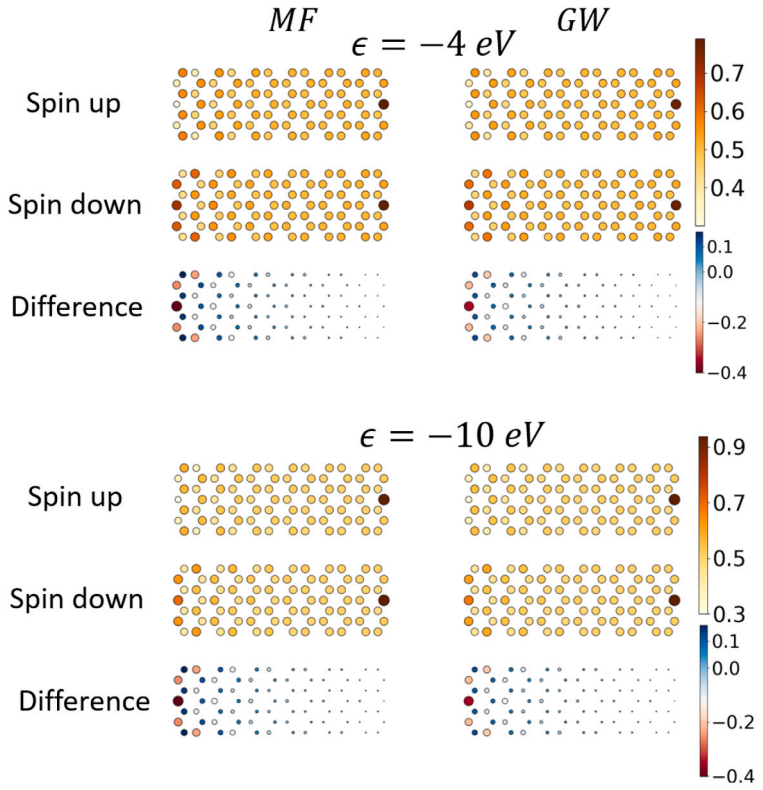

Fig. 5. Local electronic densities for one end-modified 6 UC 7-AGNRs. The left (resp., right) column shows the MF (resp., GW) results for spin up and spin down electrons (top and middle plots respectively) as well as the difference between the two spin densities (bottom plots). We used $t = 2.7$ eV and $U = 2t$.

Overall, while magnetic moments at the site of the modification strongly depend on the modification itself both in the MF and GW approximations, the correlated magnetic moments induced in the GW approximation (located at along all edges in the H-passivated case) appear to be robust to end modifications. They remain located at the unmodified edges and with a similar strength upon one- or two-end modifications for the different on-site potentials.

6. Conclusion

We conducted an investigation on the impact of end-modifications on finite-size 7-AGNRs. Our study began with a comparative analysis of various methods used in the literature to model dihydrogenation within both a tight-binding (TB) and Hubbard model frameworks. In particular, we found that adopting the *C-on-site* method yielded results akin to those obtained with the *C-removing* and *H-orbitals* methods concerning properties such as bulk-states bandgap (BS gaps), density of states (DOS), and electronic densities.

Subsequently, with a focus on the *C-on-site method*, we examined the local magnetic moments within unmodified and end-modified AGNRs. For unmodified AGNRs, our findings align with a previous study that calculated magnetic moments in GNR heterojunctions [36]. The MF approximation predicts substantial magnetic moments only in regions where topological electronic structures are located, whereas the GW approximation predicts substantial magnetic moments along all edges. Additionally, we observed that edge-localized correlated magnetic moments remain robust even when end-modifications were introduced to the AGNRs, provided that the modifications were applied solely to the unaltered edges. In contrast, magnetic moments at the locations of topological electronic structures vanish when electrons were

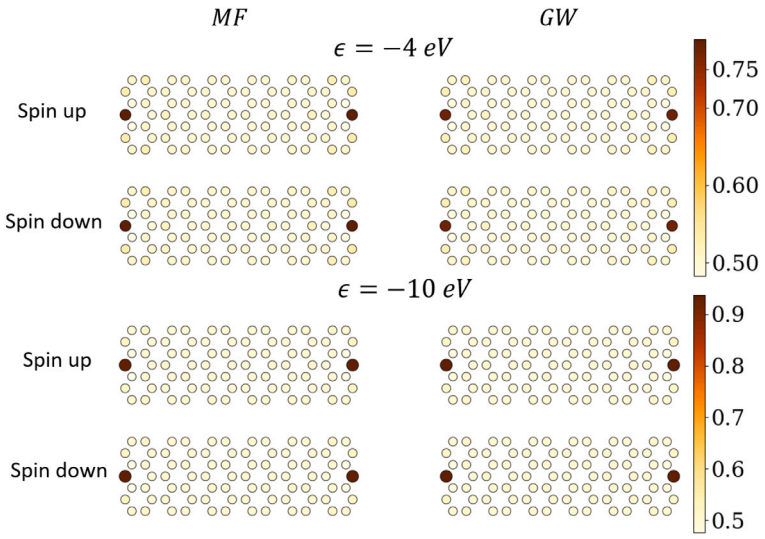

Fig. 6. Local electronic densities for two end-modified 6 UC 7-AGNRs. The left (resp., right) column shows MF (resp., GW) results for spin-up and spin-down electrons (top and bottom plots respectively). Compared to Fig. 5, the difference between spin-up and spin-down densities is not shown because it is zero everywhere (the densities are spin-symmetric).

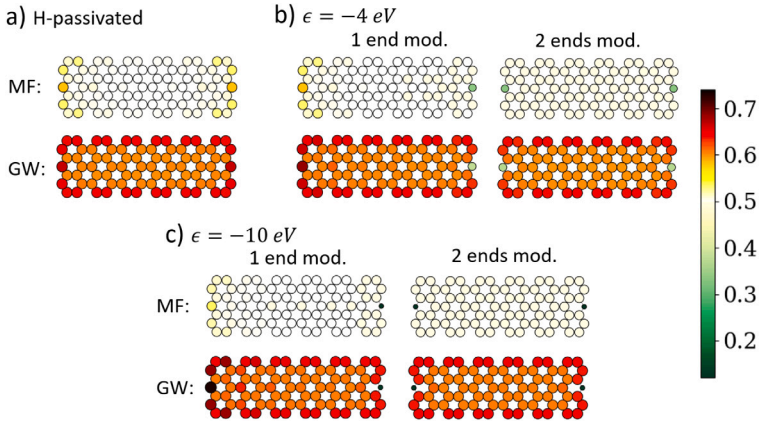

Fig. 7. Local magnetic moments for H-passivated (a) and for the one and two end-modified 6 UC 7-AGNRs with $\epsilon = -4$ eV (b) and $\epsilon = -10$ eV (c). In each case, the top (resp., bottom) illustrations correspond to the MF (resp., GW) results. In (b) and (c), the one (resp., two) end-modified cases are shown on the left (resp. right).

introduced into the system, leading to the occupation of previously unoccupied topological electronic structures in the case of H-passivated terminations.

These finite-size systems, synthesized experimentally, hold significant potential for future electrical and magnetic applications. However, given that they can be synthesized with various terminations, it is imperative to elucidate which properties are susceptible to termination-induced changes (*e.g.*, the BS gap) and which exhibit resilience (*e.g.*, local magnetic moments). The localized magnetic moments discussed here, including on-site spin–spin correlation (see Eq. (11)), have however never been reported experimentally at atomic precision for any graphene nanosystem. We hope that this will be possible in the future to confirm or refute our theoretical predictions.

CRediT authorship contribution statement

Antoine Honet: Writing – review & editing, Writing – original draft, Visualization, Software, Methodology, Investigation, Formal analysis, Data curation, Conceptualization. **Luc Henrard:** Writing – review & editing, Validation, Supervision, Methodology, Funding acquisition, Formal analysis, Conceptualization. **Vincent Meunier:** Writing – review & editing, Validation, Supervision, Methodology, Formal analysis, Conceptualization.

Declaration of competing interest

The authors declare that they have no known competing financial interests or personal relationships that could have appeared to influence the work reported in this paper.

Data availability

Data will be made available on request.

Acknowledgments

A.H. is a Research Fellow of the Fonds de la Recherche Scientifique - FNRS. This research used resources of the “Plateforme Technologique de Calcul Intensif (PTCI)” (http://www.ptci.unamur.be) located at the University of Namur, Belgium, and of the Université catholique de Louvain (CISM/UCL) which are supported by the F.R.S.-FNRS, Belgium under the convention No. 2.5020.11. The PTCI and CISM are member of the “Consortium des Équipements de Calcul Intensif (CÉCI)” (http://www.ceci-hpc.be).

Appendix A. Supplementary data

Supplementary material related to this article can be found online at https://doi.org/10.1016/j.cartre.2024.100377. It contains information on the effective representation (H-orbital case) and complementary results as the electron doping case.

References

[1] Y.-W. Son, M.L. Cohen, S.G. Louie, Energy gaps in graphene nanoribbons, Phys. Rev. Lett. 97 (21) (2006) 216803.
[2] L. Brey, H.A. Fertig, Electronic states of graphene nanoribbons studied with the Dirac equation, Phys. Rev. B 73 (23) (2006) 235411.
[3] L. Yang, C.-H. Park, Y.-W. Son, M.L. Cohen, S.G. Louie, Quasiparticle energies and band gaps in graphene nanoribbons, Phys. Rev. Lett. 99 (18) (2007) 186801.
[4] O.V. Yazyev, Emergence of magnetism in graphene materials and nanostructures, Rep. Progr. Phys. 73 (5) (2010) 056501.
[5] Y. Lu, S. Wei, J. Jin, W. Lu, L. Wang, Competition of edge effects on the electronic properties and excitonic effects in short graphene nanoribbons, New J. Phys. 18 (12) (2016) 123033.
[6] I. Hagymasi, O. Legeza, Entanglement, excitations and correlation effects in narrow zigzag graphene nanoribbons, Phys. Rev. B 94 (16) (2016) 165147.
[7] A. Honet, L. Henrard, V. Meunier, Correlation effects on topological end-states in finite-size graphene nanoribbons in the GW approximation, J. Phys.: Condens. Matter 35 (2023) 485703.
[8] P. Ruffieux, J. Cai, N.C. Plumb, L. Patthey, D. Prezzi, A. Ferretti, E. Molinari, X. Feng, K. Müllen, C.A. Pignedoli, R. Fasel, Electronic structure of atomically precise graphene nanoribbons, ACS Nano 6 (8) (2012) 6930–6935.
[9] L. Talirz, H. Söde, J. Cai, P. Ruffieux, S. Blankenburg, R. Jafaar, R. Berger, X. Feng, K. Müllen, D. Passerone, R. Fasel, C.A. Pignedoli, Termini of bottom-up fabricated graphene nanoribbons, J. Am. Chem. Soc. 135 (6) (2013) 2060–2063.
[10] H. Zhang, H. Lin, K. Sun, L. Chen, Y. Zagranyarski, N. Aghdassi, S. Duhm, Q. Li, D. Zhong, Y. Li, K. Müllen, H. Fuchs, L. Chi, On-surface synthesis of rylene-type graphene nanoribbons, J. Am. Chem. Soc. 137 (12) (2015) 4022–4025.
[11] A. Kimouche, M.M. Ervasti, R. Drost, S. Halonen, A. Harju, P.M. Joensuu, J. Sainio, P. Liljeroth, Ultra-narrow metallic armchair graphene nanoribbons, Nature Commun. 6 (1) (2015) 10177.
[12] H. Söde, L. Talirz, O. Gröning, C.A. Pignedoli, R. Berger, X. Feng, K. Müllen, R. Fasel, P. Ruffieux, Electronic band dispersion of graphene nanoribbons via Fourier-transformed scanning tunneling spectroscopy, Phys. Rev. B 91 (4) (2015) 045429.
[13] S. Wang, L. Talirz, C.A. Pignedoli, X. Feng, K. Müllen, R. Fasel, P. Ruffieux, Giant edge state splitting at atomically precise graphene zigzag edges, Nature Commun. 7 (1) (2016) 11507.
[14] L. Talirz, H. Söde, T. Dumslaff, S. Wang, J.R. Sanchez-Valencia, J. Liu, P. Shinde, C.A. Pignedoli, L. Liang, V. Meunier, N.C. Plumb, M. Shi, X. Feng, A. Narita, K. Müllen, R. Fasel, P. Ruffieux, On-surface synthesis and characterization of 9-atom wide armchair graphene nanoribbons, ACS Nano 11 (2) (2017) 1380–1388.
[15] L. Talirz, H. Söde, S. Kawai, P. Ruffieux, E. Meyer, X. Feng, K. Müllen, R. Fasel, C.A. Pignedoli, D. Passerone, Band gap of atomically precise graphene nanoribbons as a function of ribbon length and termination, ChemPhysChem 20 (18) (2019) 2348–2353.
[16] J. Lawrence, P. Brandimarte, A. Berdonces-Layunta, M.S.G. Mohammed, A. Grewal, C.C. Leon, D. Sánchez-Portal, D.G. de Oteyza, Probing the magnetism of topological end states in 5-armchair graphene nanoribbons, ACS Nano 14 (4) (2020) 4499–4508.
[17] A.H. Castro Neto, F. Guinea, N.M.R. Peres, K.S. Novoselov, A.K. Geim, The electronic properties of graphene, Rev. Modern Phys. 81 (1) (2009) 109–162.
[18] T. Cao, F. Zhao, S.G. Louie, Topological phases in graphene nanoribbons: Junction states, spin centers, and quantum spin chains, Phys. Rev. Lett. 119 (7) (2017) 076401.
[19] M.P. López-Sancho, M.C. Muñoz, Topologically protected edge and confined states in finite armchair graphene nanoribbons and their junctions, Phys. Rev. B 104 (24) (2021) 245402.
[20] J. Jiang, S.G. Louie, Topology classification using chiral symmetry and spin correlations in graphene nanoribbons, Nano Lett. 21 (1) (2021) 197–202.
[21] D. Soriano, N. Leconte, P. Ordejón, J.-C. Charlier, J.-J. Palacios, S. Roche, Magnetoresistance and magnetic ordering fingerprints in hydrogenated graphene, Phys. Rev. Lett. 107 (1) (2011) 016602.
[22] S. Kawai, S. Saito, S. Osumi, S. Yamaguchi, A.S. Foster, P. Spijker, E. Meyer, Atomically controlled substitutional boron-doping of graphene nanoribbons, Nature Commun. 6 (1) (2015) 8098.
[23] R.R. Cloke, T. Marangoni, G.D. Nguyen, T. Joshi, D.J. Rizzo, C. Bronner, T. Cao, S.G. Louie, M.F. Crommie, F.R. Fischer, Site-specific substitutional boron doping of semiconducting armchair graphene nanoribbons, J. Am. Chem. Soc. 137 (28) (2015) 8872–8875.
[24] S. Kawai, S. Nakatsuka, T. Hatakeyama, R. Pawlak, T. Meier, J. Tracey, E. Meyer, A.S. Foster, Multiple heteroatom substitution to graphene nanoribbon, Sci. Adv. 4 (4) (2018) eaar7181.
[25] S. Latil, S. Roche, D. Mayou, J.-C. Charlier, Mesoscopic transport in chemically doped carbon nanotubes, Phys. Rev. Lett. 92 (25) (2004) 256805.
[26] H. Khalfoun, P. Hermet, L. Henrard, S. Latil, B and N codoping effect on electronic transport in carbon nanotubes, Phys. Rev. B 81 (19) (2010) 193411.
[27] P. Lambin, H. Amara, F. Ducastelle, L. Henrard, Long-range interactions between substitutional nitrogen dopants in graphene: Electronic properties calculations, Phys. Rev. B 86 (4) (2012) 045448.
[28] H. Khalfoun, P. Lambin, L. Henrard, Long-range resonant effects on electronic transport of nitrogen-doped carbon nanotubes, Phys. Rev. B 89 (4) (2014) 045407.
[29] F. Joucken, Y. Tison, P. Le Fèvre, A. Tejeda, A. Taleb-Ibrahimi, E. Conrad, V. Repain, C. Chacon, A. Bellec, Y. Girard, S. Rousset, J. Ghijsen, R. Sporken, H. Amara, F. Ducastelle, J. Lagoute, Charge transfer and electronic doping in nitrogen-doped graphene, Sci. Rep. 5 (1) (2015) 14564.
[30] J. Fernández-Rossier, J.J. Palacios, Magnetism in graphene nanoislands, Phys. Rev. Lett. 99 (17) (2007) 177204.
[31] H. Kumazaki, D.S. Hirashima, Tight-binding study of nonmagnetic-defect-induced magnetism in graphene, Low Temp. Phys. 34 (10) (2008) 805–811.
[32] N.A. Pike, D. Stroud, Tight-binding model for adatoms on graphene: Analytical density of states, spectral function, and induced magnetic moment, Phys. Rev. B 89 (11) (2014) 115428.
[33] S. Mishra, D. Beyer, K. Eimre, S. Kezilebieke, R. Berger, O. Gröning, C.A. Pignedoli, K. Müllen, P. Liljeroth, P. Ruffieux, X. Feng, R. Fasel, Topological frustration induces unconventional magnetism in a nanographene, Nature Nanotechnology 15 (1) (2020) 22–28.
[34] H. Feldner, Z.Y. Meng, A. Honecker, D. Cabra, S. Wessel, F.F. Assaad, Magnetism of finite graphene samples: Mean-field theory compared with exact diagonalization and quantum Monte Carlo simulations, Phys. Rev. B 81 (11) (2010) 115416.
[35] M. Raczkowski, F.F. Assaad, Interplay between the edge-state magnetism and long-range Coulomb interaction in zigzag graphene nanoribbons: Quantum Monte Carlo study, Phys. Rev. B 96 (11) (2017) 115155.
[36] J.-P. Joost, A.-P. Jauho, M. Bonitz, Correlated topological states in graphene nanoribbon heterostructures, Nano Lett. 19 (12) (2019) 9045–9050.
[37] M. Raczkowski, R. Peters, T.T. Phùng, N. Takemori, F.F. Assaad, A. Honecker, J. Vahedi, Hubbard model on the honeycomb lattice: From static and dynamical mean-field theories to lattice quantum Monte Carlo simulations, Phys. Rev. B 101 (12) (2020) 125103.
[38] A. Honet, L. Henrard, V. Meunier, Exact and many-body perturbation solutions of the Hubbard model applied to linear chains, AIP Adv. 12 (3) (2022) 035238.
[39] A. Honet, L. Henrard, V. Meunier, Semi-empirical many-body formalism of optical absorption in nanosystems and molecules, Carbon Trends 4 (2021) 100073.
[40] T.O. Wehling, S. Yuan, A.I. Lichtenstein, A.K. Geim, M.I. Katsnelson, Resonant scattering by realistic impurities in graphene, Phys. Rev. Lett. 105 (5) (2010) 056802.
[41] Z. Bullard, E.C. Girão, J.R. Owens, W.A. Shelton, V. Meunier, Improved all-carbon spintronic device design, Sci. Rep. 5 (1) (2015) 7634.
[42] S. Mishra, D. Beyer, K. Eimre, R. Ortiz, J. Fernández-Rossier, R. Berger, O. Gröning, C.A. Pignedoli, R. Fasel, X. Feng, P. Ruffieux, Collective all-carbon magnetism in triangulene dimers**, Angew. Chem. Int. Ed. 59 (2020) 12041.
[43] A. Honet, L. Henrard, V. Meunier, Mean-field approximation of the Fermi–Hubbard model expressed in a many-body basis, AIP Adv. 13 (7) (2023) 075210.
[44] L. Hedin, S. Lundqvist, Effects of electron-electron and electron-phonon interactions on the one-electron states of solids, in: F. Seitz, D. Turnbull, H. Ehrenreich (Eds.), in: Solid State Physics, vol. 23, Academic Press, 1970, pp. 1–181.
[45] G. Stefanucci, R. van Leeuwen, Nonequilibrium Many-Body Theory of Quantum Systems: A Modern Introduction, Cambridge University Press, Cambridge, 2013.
[46] J.-P. Joost, N. Schlünzen, S. Hese, M. Bonitz, C. Verdozzi, P. Schmitteckert, M. Hopjan, Löwdin's symmetry dilemma within green functions theory for the one-dimensional hubbard model, Contrib. Plasma Phys. (2021) e202000220.
[47] A. Honet, Hubbard_GW (v1.0), Zenodo (2023) http://dx.doi.org/10.5281/zenodo.8380028.
[48] D. Moldovan, M. Andelkovic, F. Peeters, pybinding v0.9.5: a Python package for tight- binding calculations, Zenodo (2020) http://dx.doi.org/10.5281/zenodo.4010216.
[49] M.R. Zirnbauer, Particle–hole symmetries in condensed matter, J. Math. Phys. 62 (2) (2021) 021101.
[50] D.P. Arovas, E. Berg, S.A. Kivelson, S. Raghu, The Hubbard Model, Annu. Rev. Condens. Matter Phys. 13 (2022) 239–274.